

Quasifission and Shell Effects in Reactions Forming ^{266}Sg

A. Wakhle^{1,a}, D.J. Hinde¹, M. Dasgupta¹, R. du Rietz¹, C. Simenel², M. Evers¹, D.H. Luong¹, and R. Rafiei¹

¹ Department of Nuclear Physics, Research School of Physics and Engineering, Australian National University, Canberra, Australian Capital Territory 0200, Australia

² CEA, Centre de Saclay, IRFU/Service de Physique Nuclaire, F-91191 Gif-sur-Yvette, France

Abstract. The role of shell effects in reactions forming the heavy element ^{266}Sg was investigated using the Mass Angle Distribution technique. For the $^{34}\text{S} + ^{232}\text{Th}$ reaction the doubly magic shell closure at ^{208}Pb was found to strongly influence asymmetric quasifission, the exit channel at sub barrier energies. The evolution of the dinuclear system is arrested as it passes through this mass region. Mass splits corresponding to $A_L/A_H \approx 58/208$ are seen for a large range of angles indicating a long timescale for this process. The more mass asymmetric $^{28}\text{Si} + ^{238}\text{U}$ reaction has a much smaller quasifission cross section. Therefore the shell effects around ^{208}Pb are not dominant here.

1 Introduction

Recent work on near barrier collisions of heavy nuclei is driven by a strong interest in the synthesis of superheavy elements to study the predicted 'island of stability' resulting from predicted shell closures at neutron number 184 and proton numbers between 114 to 126 [1,2].

Forming and detecting superheavy elements is a very difficult task as a consequence of their minuscule (pico barn to sub-pico barn) formation cross sections. In practice superheavy elements can only be formed by fusing two massive nuclei. Using a particle accelerator they are brought into contact by providing them with kinetic energy sufficient to overcome their mutual Coulomb repulsion. However, fusion is not the most likely outcome. The reaction outcome is dominated by the reseparation of the elongated dinuclear system prior to fusion. This process is called quasifission and is a competitor to fusion. Even after fusion, the excited compound nucleus (CN) is extremely likely to undergo fission instead of reaching the ground state of a superheavy nucleus. This process is called fusion-fission.

The relationship between quasifission and fusion-fission is an important aspect of nuclear reaction dynamics. Previous work [3] has inferred that the lifetime of these two processes is vastly different (10^{-20} - 10^{-21} s and $\sim 10^{-18}$ s, respectively). However, disentangling these two processes is not always easy since their observable characteristics may overlap considerably.

The reaction dynamics of heavy ion reactions depend on several parameters such as mass, charge, deformation orientation and shell structure of the colliding nuclei, entrance channel mass asymmetry and collision energy. Prior work has shown that the competition between fusion-fission and quasifission is affected by shell driven deformation and orientation [4–8]. In this work we show that the quasifission process is strongly influenced by shell effects encountered during the evolution of the dinuclear system.

^a e-mail: aditya.wakhle@anu.edu.au

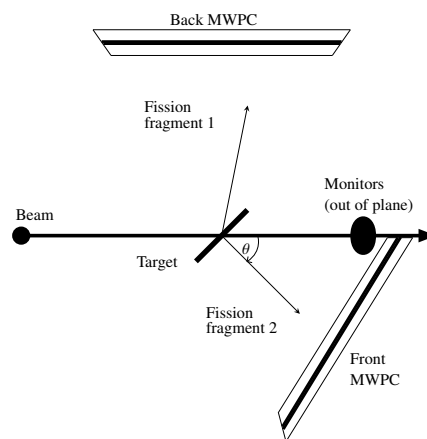


Fig. 1. Configuration of the MWPCs used in the experiments.

Historically several techniques have been employed to disentangle fusion-fission from quasifission. In [4] the Mass Distribution of Fission Fragments (MDFF) technique is used to separate exit channels based on outgoing fragment mass. In [9] the Mass Energy Distribution (MED) technique separates reaction channels based on the total kinetic energy of the outgoing fragments. We employ the Mass Angle Distribution (MAD) technique [3,5,6,10,11] to study heavy ion reactions. This involves measuring the angular distribution and mass of fragments from a reaction. Quasifission has two typical signatures; a large angular anisotropy and a wide mass distribution or a large mass-asymmetry leading to a separate component in mass altogether with a focused angular distribution. Fusion-fission gives a mass distribution about symmetric masses with an isotropic angular distribution.

2 Experimental Details

To isolate effects of the entrance channel two reactions were measured forming the same CN. The measurements

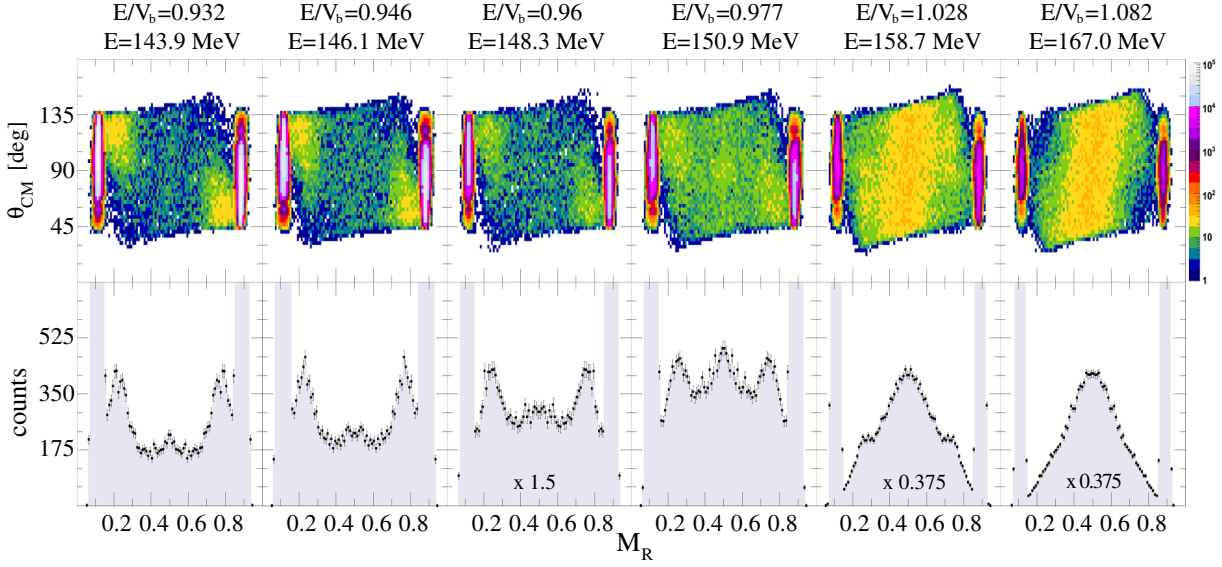


Fig. 2. (Colour online). Mass angle distributions for full momentum transfer (FMT) events in the reaction $^{34}\text{S} + ^{232}\text{Th}$ ($V_{B,cm} = 154.4$ MeV). The lower frames show the corresponding projected mass-ratio distributions. The mass-asymmetric component is significant at $E/V_B > 1$ and is the dominant reaction channel for $E/V_B < 1$.

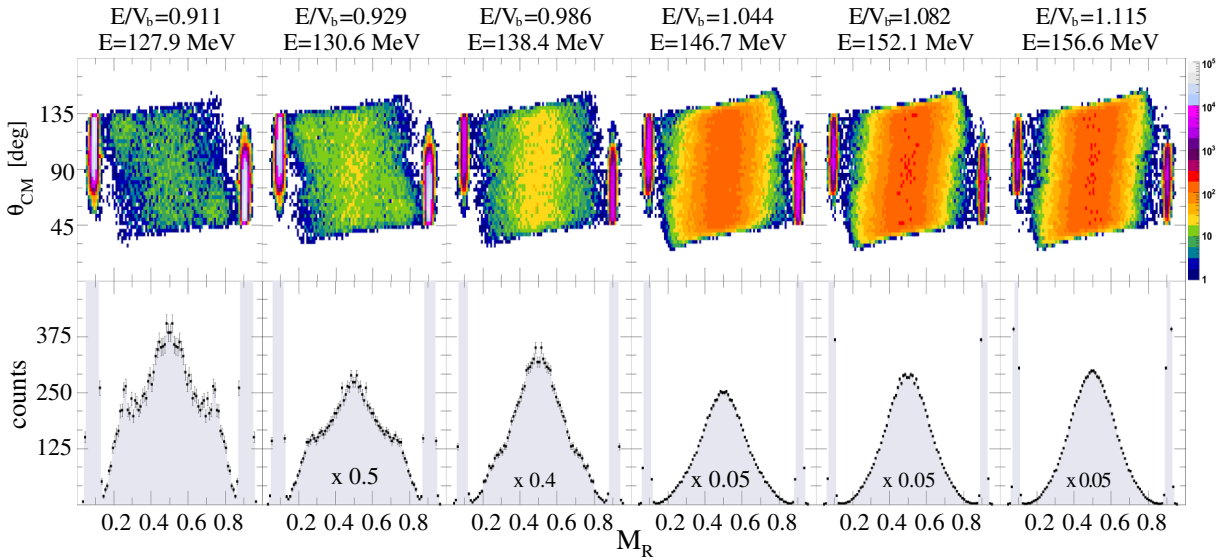


Fig. 3. (Colour online). Mass angle distributions for FMT events in the reaction $^{28}\text{Si} + ^{238}\text{U}$ ($V_{B,cm} = 140.5$ MeV). Mass-symmetric fission is the dominant reaction channel for $E/V_B > 1$ and mass-asymmetric fission, consistent with quasi-fission, is clearly seen at $E/V_B < 1$. The MAD's also show a slight mass angle correlation for the more mass-symmetric component.

forming the CN ^{266}Sg were conducted using pulsed beams of ^{28}Si and ^{34}S from the 14UD tandem electrostatic accelerator at the Australian National University. For all beams the pulsing provided a separation of 106.3 ns between pulses with FWHM of ≈ 1 ns. Targets of ^{232}Th and $^{238}\text{UF}_4$ were used for the reactions of interest and targets of ^{208}PbS and ^{197}Au were used for calibration. The first three targets had a ^{12}C backing of thickness $\approx 15 \mu\text{g cm}^{-2}$ while the ^{197}Au target was self supporting.

Reaction products were detected using two large area position sensitive Multiwire Proportional Counters (MWPCs). Each detector had an active area spanning 284 mm in width and 357 mm in height. A grid of position sensitive wires provided a spatial resolution of 1 mm. As illustrated in figure 1, the detectors were placed 180 mm from the target and covered the forward angles $5^\circ \leq \theta_{lab} \leq 80^\circ$ and backward angles $55^\circ \leq \theta_{lab} \leq 130^\circ$. The data acquisition

system was triggered when both counters measured fission fragments in coincidence. Two silicon surface-barrier detectors positioned at $\theta_{lab} = 0^\circ$ $\phi_{lab} = \pm 22^\circ$, were used as monitors to measure elastic scattering events for cross section normalisation.

The fragment velocity vectors are determined using the position and timing information from the MWPCs. The mass ratio (M_R) is defined as:

$$M_R = \frac{A_2}{A_1 + A_2} = \frac{V_1}{V_1 + V_2} \quad (1)$$

where A_i represents the masses of each fragment i . Displaying the mass ratio as a function of scattering angle $\theta_{c.m.}$ produces a mass angle distribution. The details of the analysis procedure are presented in [6].

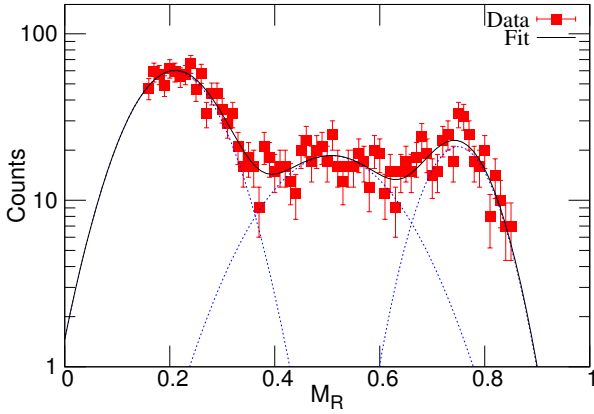


Fig. 4. (Colour online). An example of a fit to the mass distributions. The dotted lines correspond to individual Gaussian functions while the solid line is the overall fit.

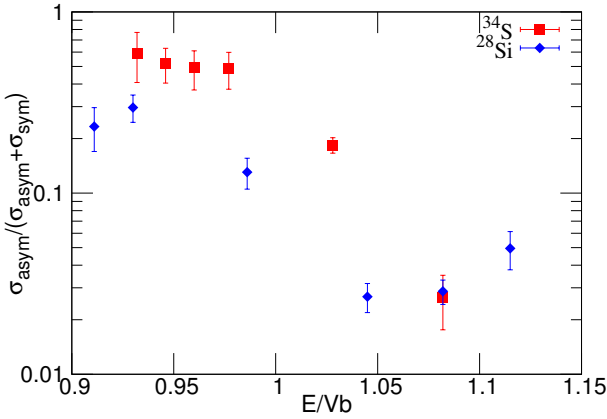


Fig. 5. (Colour online). Relative yield of the asymmetric and symmetric mass components for both reactions with respect to E/V_b .

3 Results

Figures 2 and 3 show the mass angle distributions for all the measured energies (E_{cm}) for the ^{34}S and ^{28}Si induced reactions respectively. We detect binary events and record information for both the fission fragments. Each point in the MADs has a corresponding point at a centre-of mass angle of $180^\circ - \theta_{cm}$ and at a mass ratio of $1 - M_R$. This makes visual identification any mass angle correlations easier.

Figures 2 and 3 both show two distinct components in the MADs and the mass projections. At energies below the barrier we see a mass asymmetric component that is strongly focused at forward and backward angles. At energies above the barrier we see a more mass-symmetric component with an angular distribution tending to symmetry around $\theta_{cm} = 90^\circ$.

To quantify the differences between the two reactions, the mass ratio projections for all data sets were fitted with up to three overlapping Gaussian functions. The widths and centroids of the Gaussians were not constrained. Figure 4 shows a typical fit of three overlapping Gaussians to the mass projections. The peaks were not expected to be Gaussian. The use of Gaussians here is justified by the need to quantify the position of the peaks, estimate the average mass of the fragments and the area under a given peak in a systematic manner.

Figure 5 depicts the fraction of the asymmetric component as a function of energy with respect to the barrier. The mass asymmetric fission peaks correspond to mass asymmetric quasifission while the symmetric fission peaks correspond to either fusion-fission or more mass-symmetric quasifission. The overlap of the latter two reaction channels has been covered in prior work [10, 11] and will be discussed only briefly.

From figures 2, 3 and 5 we see that for both reactions there is a strong mass asymmetric quasifission component at sub barrier energies. Both reactions also have a small mass asymmetric component at energies above the barrier. The mass asymmetric quasifission yield varies significantly between the two reactions. The ^{34}S induced reaction has a much stronger component as compared to the ^{28}Si induced reaction. This is because the quasifission cross section decreases with increasing mass asymmetry of the entrance channel. This dependence on entrance channel mass asymmetry is a well studied phenomenon [12].

Fusion-fission events are expected to lie around $M_R = 0.5$ and exhibit an angular distribution symmetric around $\theta_{cm} = 90^\circ$. However, at the highest energies the mass angle distributions for both reactions measured show a correlation between the mass ratio and the centre-of-mass angle. This is characterised by an anisotropic distribution around $M_R = 0.5$. Fission like events furthest from symmetry are found at forward and backward angles. Previous work [11] has shown that these events are quasifission taking place at time scales significantly longer than 10^{-21}s . The MAD technique is extremely sensitive to the shortest reaction time scales. Therefore there is a significant overlap between fusion-fission and mass-symmetric quasifission. Nonetheless, the large anisotropies confirm that quasifission is a dominant exit channel even at the highest energies.

Figure 6 shows the masses of the asymmetric (light) and symmetric peaks vs. energy for both reactions. It is sufficient to look at only the light and symmetric peaks since the heavy peak corresponds to the complementary target like fragment and reveals no additional information.

On average the asymmetric splits observed in the ^{34}S induced reactions correspond to a light-heavy fragment mass of 58-208u. This indicates that the doubly magic shell closure at ^{208}Pb might be playing a role in the outcome of the asymmetric reaction channel. The ^{28}Si induced reaction has a slightly more symmetrised light-heavy fragment mass of 68-198u. The highest energies do not have an asymmetric component consistent with the trend seen in figure 5. The sensitivity to any shell effects is expected to diminish with increasing excitation energy.

Following contact (for non-central collisions) the dinuclear system begins rotating and the angle it rotates through is directly proportional to the reaction time. Thus we can relate the outgoing angle of fragments (the measured angle) to the reaction time scale. For the light fragment a backward outgoing angle corresponds to short reaction times. If the dinuclear system separates after a slightly longer contact time the outgoing angle will be more forward. This is explained in detail in [3, 11].

The ^{34}S induced reactions were studied in more detail because of the large asymmetric quasifission component at low energies and better statistics as compared to the ^{28}Si induced reactions. For the ^{34}S induced reaction the lowest

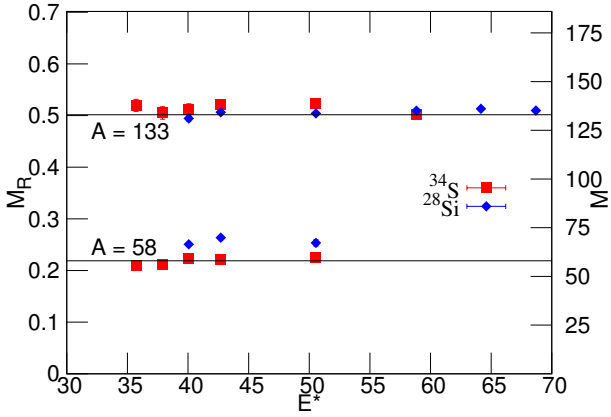


Fig. 6. (Colour online). Masses of the light and symmetric fragments for both reactions as a function of Excitation Energy E^* . The two solid lines mark $A=133$ (symmetric fission) and $A=58$ (complementary light partner for $A=208$).

3 energies were summed to boost statistics and 5° cuts in centre of mass scattering angle were made. For each angular cut the mass projections were fitted with up to three overlapping Gaussians as described earlier. Figure 7 shows the mass ratio of the light and symmetric peaks vs. scattering angle obtained from these fits. Note that the error bars correspond to the widths (σ) of the respective peaks and do not overlap.

In the absence of a shell closure we expect a smooth evolution of the (light fragment) mass from asymmetric splits at the most backward angles to more symmetric splits at forward angles. That is, the dinuclear system exchanges more and more mass as it rotates through a larger angle and stays in contact for a longer duration. An example of this can be seen in [11] for reactions of ^{48}Ti with W targets.

In figure 7, at the most backward angles the fragments correspond to the nucleus ^{58}Cr (assuming N/Z equilibration takes place early on in the collision [13]) which is the complimentary light partner of ^{208}Pb . At the most forward angles the fragments correspond to ^{69}Co and ^{197}Au . Overall the average mass splits correspond to a light-heavy fragment mass of 62-204u. The mass drift from $A = 208$ to $A = 197$ varies only slightly with respect to scattering angle. Thus the system exhibits a very strong tendency of splitting into two fragments with the heavier being in the $A = 208$ region. Since the outgoing angle is directly correlated with the interaction time of the dinuclear system this implies that once the dinucleus reaches the ^{208}Pb - ^{58}Cr configuration the mass drift is arrested. This indicates that the doubly magic shell closure at ^{208}Pb plays a strong role in the evolution of the dinuclear system.

4 Conclusion

The reactions $^{34}\text{S} + ^{232}\text{Th}$ and $^{28}\text{Si} + ^{238}\text{U}$, both forming the compound nucleus ^{266}Sg , were studied using the Mass Angle Distribution technique. Based on the MADs and mass projections quasifission was found to be a dominant exit channel in both reactions. The masses of the asymmetric quasifission fragments suggested that shell effects around the doubly magic ^{208}Pb nucleus strongly influence the reaction dynamics. A detailed investigation of the

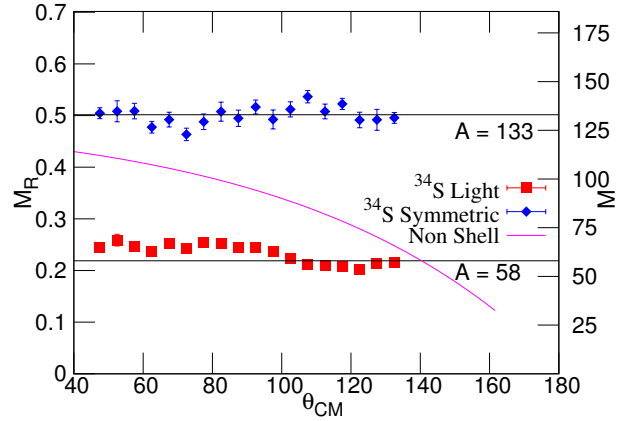


Fig. 7. (Colour online). Masses of the light and symmetric fragments measured for the $^{34}\text{S} + ^{232}\text{Th}$ reaction vs. centre of mass scattering angle. The error bars are the widths (σ) of the respective peaks. The uncertainties on the centroids are on average as big as the points. The two solid lines mark $A=133$ (symmetric fission) and $A=58$ (complementary light partner for $A=208$). The curved line depicts the expected mass evolution of the light peak in the absence of any shell effects.

^{34}S induced reactions over a large range of angles found that the mass splits vary only slightly around $A=208$ with outgoing angle. The direct proportionality between angle and contact time confirmed that the doubly magic ^{208}Pb shell closure does indeed affect the quasifission exit channel very strongly. This shell effect was also observed in [14]. This effect was not as strong in the $^{28}\text{Si} + ^{238}\text{U}$ reactions due to a smaller quasifission cross section.

References

1. Y.T. Oganessian, et al., Phys. Rev. C **74** 044602 (2006)
2. S. Hofmann, et al., Eur. Phys. J. A **32** 251 (2007)
3. J. Töke et al., Nucl. Phys. A **440**, 327-365 (1985)
4. K. Nishio et al., Phys. Rev. C **82**, 044604 (2008)
5. D.J. Hinde et al., Phys. Rev. Lett. **101**, 202701 (2008)
6. D.J. Hinde et al., Phys. Rev. C **53**, 1290 (1996)
7. Y.T. Oganessian, et al., Phys. Rev. C **70** 064609 (2004)
8. D.J. Hinde, et al., Phys. Rev. Lett. **74** 1295 (1995)
9. M.G. Itkis et al., Nucl. Phys. A **734**, 136-147 (2004)
10. D.J. Hinde et al., Phys. Rev. Lett. **101**, 092701 (2008)
11. R. du Rietz et al., Phys. Rev. Lett. **106**, 052701 (2011)
12. M. Dasgupta and D.J. Hinde, Nucl. Phys. A **734**, 148-155 (2004)
13. C. Simenel et al., Phys. Lett. B **710**, 607-611 (2012)
14. M.G. Itkis et al., Fusion Dynamics At The Extremes, pp. 93-109 (2001)